The effect of poly(ethylene glycol) coating and monomer type on poly(alkyl cyanoacrylate) nanoparticle interactions with lipid monolayers and cells

Habib Baghirov[a*], *Sopio Melikishvili*[b], *Yrr Mørch*[c], *Einar Sulheim*[a,c], *Andreas Åslund*[a], *Tibor Hianik*[b‡], *Catharina de Lange Davies*[a‡]

[a]Department of Physics, The Norwegian University of Science and Technology (NTNU), 7491 Trondheim, Norway

[b]Faculty of Mathematics, Physics and Informatics, Comenius University, 84248 Bratislava, Slovakia

[c]SINTEF Materials and Chemistry, 7465 Trondheim, Norway

‡These authors contributed equally

*Tel.: +4773593492. Email: habib.baghirov@ntnu.no

The authors declare no competing financial interest.

This manuscript contains 5976 words excluding the abstract and references. The combined number of tables and figures in the manuscript is 8.

Graphical Abstract

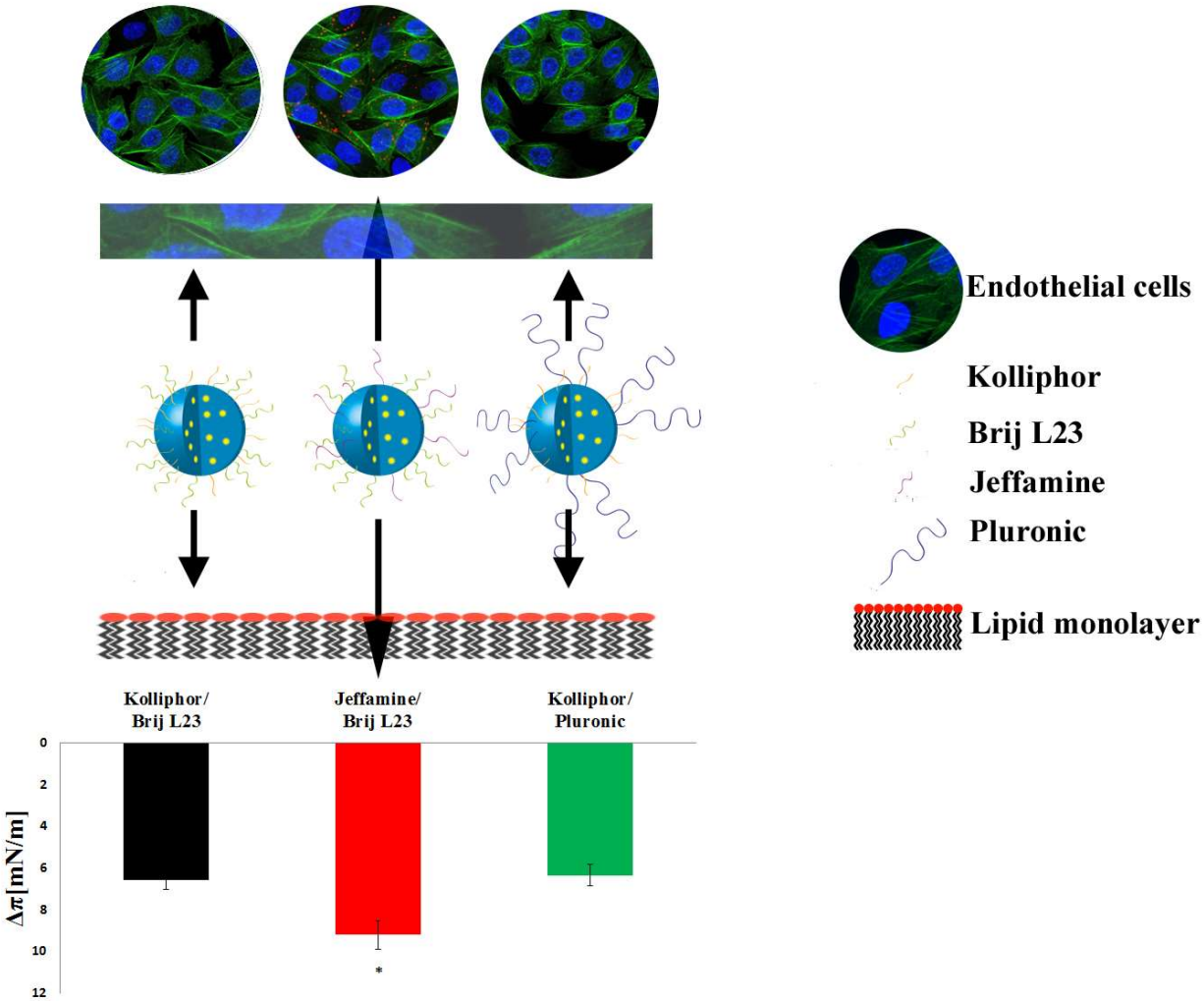

Abstract

The interaction of the promising drug carriers poly(alkyl cyanoacrylate) nanoparticles (PACA NPs) with lipid monolayers modeling the cell membrane and with RBE4 immortalized rat brain endothelial cells was compared to assess the relevance of lipid monolayer-based cell membrane models for PACA NP cellular uptake. NP properties such as size and charge of NPs and density of poly(ethylene glycol) coating (PEG) were kept in a narrow range to assess whether the type of PEG coating and the PACA monomer affected NP-monolayer and NP-cell interactions.

The interaction with lipid monolayers was evaluated using surface pressure measurements and Brewster angle microscopy. NP association with and uptake by cells were assessed using flow cytometry and confocal laser scanning microscopy.

The interaction between NPs and both lipid monolayers and the plasma membrane depended on the type of PEG. PEG density affected cellular uptake but not interaction with lipid monolayers. NP monomer, NPs size and charge had no effect on the interaction. This might be due to the fact that the size and charge distribution was kept rather narrow to study the effect of PACA monomer and PEG type.

In conclusion, while modeling solely the passive aspect of NP-cell interactions, lipid monolayers nevertheless proved a valuable cell membrane model whose interaction with PACA NPs correlated well with NP-cell interaction. In addition, both NP-monolayer and NP-cell interaction were dependent on PEGylation type, which could be used in the design of NPs to either facilitate or hinder cellular uptake, depending on the intended purpose.

Keywords: poly(alkyl cyanoacrylate) nanoparticles, lipid monolayers, nanoparticle-cell interactions, cellular uptake, poly(ethylene glycol)

1. Introduction

Nanoparticles (NPs) have emerged as promising drug carriers owing to their ability to accumulate in tumor tissues due to the enhanced permeability and retention effect [1], potential for functionalization with moieties that increase cellular uptake of NPs, and ensuring sustained and controlled release of drugs [2, 3]. Uptake of NPs by living cells depends on various physico-chemical properties of the NPs such as NP size [4-6], aspect ratio [4, 7], charge [5, 6], hydrophobicity [8], and others.

One of the properties whose effect on NP-cell interactions is relatively poorly understood is the amount and type of poly(ethylene glycol) (PEG) coating that is commonly employed to shield NPs from the reticuloendothelial system (RES) in vivo [9]. PEGylation has been shown to extend the circulation time of NPs in blood, although it may come at the expense of reduced cellular uptake due to reduced interaction with proteins [10]. This is generally thought to be the very mechanism that protects PEGylated NPs from opsonization and interception by macrophages in vivo [11].

Poly(alkyl cyanoacrylate) NPs (PACA NPs) have shown promise in drug delivery due to the ease of their synthesis and functionalization [12], with one type of PACA NPs currently being in Phase III clinical trial for the treatment of advanced hepatocellular carcinoma [13]. The composition of PACA NPs varies depending, in particular, on the nature of the alkyl monomer and the type of surfactant (e.g. PEG) coating. Various combinations of PACA NP properties allow adjusting their degradability, circulation half-life and other parameters relevant for drug delivery and biodistribution [5, 14].

While cellular uptake of NPs is normally dominated by active processes such as endocytosis [15], passive association of NPs with the cellular membrane is the first step in the internalization

of non-targeted NPs. That association can be studied using biomimetic membrane models such as lipid monolayers comprising lipids found in the cell membrane [16]. Indeed, while lipid monolayers have commonly been used to study interactions between small molecular drugs and lipid-based cell membrane models [17], a few studies probed their interactions with NPs [18-22], showing in some instances that they can be relevant models of NP-cell interactions correlating well with NP uptake [19, 20]. NP properties that have been studied in those models include size [23], charge [18], and the presence of targeting moieties [20]. To the best of our knowledge, however, the relevance of biomimetic membrane models for NP cellular uptake has not been studied with regard to PEG coating density or type, nor have those models been applied to studies of PACA NPs. In addition, while the alkyl chain length in PACA NPs has been shown to affect NP degradability [5, 24] and cytotoxicity [25], its effect on NP uptake has received less attention and, as far as we are aware, has not been studied systematically.

We therefore investigated whether lipid monolayers could be used to model the interaction between PACA NPs and living cells, and whether this interaction was dependent on the nature of the monomer and PEG type on PACA NPs. Toward that end, we produced an array of PACA NPs with properties such as particle size, charge and PEGylation density distributed in a relatively limited range in order to identify the effects of PACA NP monomer and PEG type. The two monomer types chosen in our study were (butyl cyanoacrylate) (BCA) and (isohexyl cyanoacrylate) (IHCA), as these have been most relevant in preclinical studies and clinical trials. The artificial cell membrane was composed of a mixture of 1.2-dimyristoyl-sn-glycero-3-phosphocholine (DMPC) and 1.2-dipalmitoyl-sn-glycero-3-phosphoglycerol (DPPG) lipids commonly used in cell membrane models [22]. Rat brain endothelial cell line RBE4 was chosen for cellular association and uptake studies due to the high uptake of PACA NPs by RBE4 cells

observed in our previous study [24]. Interactions between PACA NPs and the artificial membrane were compared to PACA NP association with and uptake by RBE4 cells. We found that the lipid monolayers could be a relevant model for the cellular association and uptake of PACA NPs, and that PACA NP interactions with the artificial DMPC/DPPG membrane and RBE4 endothelial cells were affected by the type of PEG coating, while the monomer type did not significantly affect interactions in either model.

2. Experimental section

2.1. Nanoparticles

PACA NPs were synthesized using miniemulsion polymerization as previously described [26]. Briefly, the oil phase was prepared by mixing the monomer, BCA or IHCA (all from Henkel Loctite), containing a co-stabilizer (Miglyol 810N, Cremer), a radical initiator (V65, Azobisdimetyl valeronitril, Wako) and, in some NP, a fluorescent dye. The dyes used were either NR668 [27] (a kind gift from Dr. Klymchenko, University of Strasbourg), p-HTAH [28] (a kind gift from Peter Nilsson, Linköping University), or DiR (Life Technologies). The particles were PEGylated using four different non-ionic PEG-based surfactants: Brij L23 (23 ethylene glycol units, MW~1225, Sigma Aldrich), Kolliphor HS 15 (15 ethylene glycol units, MW~960, Sigma Aldrich), Pluronic F68 (triblock copolymer composed of a central hydrophobic chain of poly(propylene oxide) flanked by two PEG chains of 78 ethylene glycol units each, MW~8400, Sigma Aldrich), and Jeffamine®M-2070, 31 ethylene glycol units, MW~2000, Huntsman Corporation). The oil-in-water emulsion was made by mixing the oil phase with a water phase (0.1 M HCl) containing one non-reactive stabilizing (Brij L23 or Pluronic F68), and one reactive

initiating (Kolliphor HS 15 or Jeffamine® M-2070) PEG-based surfactant. The polymerization reaction was initiated by the amino and hydroxyl group on the lipophilic chains of Jeffamine® M-2070 and Kolliphor HS 15, respectively. Components in each batch of NPs are shown in Table 1. Polymerization was carried out for 24 hours at room temperature, followed by 8 hours at 50°C (to activate the radical initiator to ensure polymerization of any un-reacted monomer). After polymerization, the NPs were dialyzed against 1.1 μM HCl with MWCO 12-14000 Da to remove the excess of surfactants.

2.2. Nanoparticle characterization

The PEG-coated NPs were characterized for hydrodynamic size distribution, polydispersity index (PDI) and surface charge (ζ-potential) using dynamic light scattering (DLS, Zetasizer Nano ZS, Malvern Instruments) in 0.01 M phosphate buffer, pH 7. PEGylation of NPs was confirmed by 1H-nuclear magnetic resonance (NMR) using a Bruker Avance DPX 400 MHz with autosampler. Prior to NMR, the dialyzed NPs were washed with distilled water and centrifuged three times before drying at 50°C overnight. The samples were dissolved in Acetone-D6 and scanned for 32 scans. The spectra were processed in Mestrenova 9.0.1 (Mestrelab Research S.L.) and the solvent residual peak at 2.05 ppm was used as reference. To calculate PEGylation, the characteristic PEG-peaks at 3.6 ppm, the peak of a triplet from Miglyol 810N at 2.33 ppm and methylene groups of poly (alkyl cyanoacrylate) at 1.75 ppm were integrated. From the integrals, number of protons corresponding to each integral, the dry weight of the material and the size, concentration and density (1.148 g/ml) of NP, it was possible to calculate the number of ethylene units/nm^2.

2.3. Phospholipids and monolayer preparation

DMPC and DPPG lipids were purchased from Avanti Polar Lipids Inc. Their mixture with a DMPC/DPPG molar ratio of 10:1 was prepared in chloroform (Slavus) and stored at 4ºC until further use. The mixture of DMPC/DPPG lipids had a negative charge (-25.6±1.58) typical for cell membranes [29, 30]. DMPC/DPPG monolayers were prepared by homogenous deposition of DMPC/DPPG mixture droplets onto 10 ml of subphase (phosphate-buffered saline, Sigma) (PBS) pre-added to an in-house Teflon container of circular shape (volume 10 ml). The container with a pressure sensor was placed into the laminary box in order to avoid possible contamination by dust microparticles. The temperature inside the box was controlled using a thermometer. The lipid mixture was deposited using a Hamilton syringe (Hamilton Company), and surface pressure of the monolayer was monitored using a PS4 surface pressure sensor (NIMA Technology) until a required initial surface pressure value was reached. We analyzed interaction of NPs with monolayers at surface pressures 10, 20 and 30 mN/m, corresponding to the liquid-condensed (10 mN/m) and solid states (20-30 mN/m) of the monolayer. Monolayers were allowed to equilibrate under stirring at ambient temperature (T=23±1 ºC). The temperature was controlled by air conditioning in the room.

After the formation of DMPC/DPPG monolayers on the subphase, NPs were injected to the subphase at an initial concentration of 20 µg/ml using a Hamilton syringe, still under stirring and while monitoring the surface pressure using a surface pressure sensor. The initial concentration of 20 µg/ml was chosen because it was used in our previous studies on the cellular uptake of PACA NPs without any cytotoxic effect [24]. NPs were further added to the subphase to reach total concentrations of 40, 60 and 80 µg/ml once the effect on the surface pressure following the

previous NP injection had reached a plateau. Changes in the surface pressure values were calculated based on the values in such graphs.

2.4. Brewster angle microscopy

DMPG/DPPG monolayers were formed on the subphase and NPs were injected at gradually increasing concentrations as described in Section 2.3, except that a black glass plate was placed on the bottom of the in-house Teflon container to allow visualization of the interactions between NPs and the lipid monolayers with Brewster angle microscopy (BAM) (BAM 3, NIMA Technology). The BAM was equipped with a HeNe laser emitting p-polarized light with a wavelength of 659 nm that was reflected off at the air/buffer interface at the Brewster angle (53.1˚). The reflected light passed through a focal lens into an analyzer and, finally, to a CCD camera. The collection of this reflected radiation with a video camera allowed in situ, real time visualization of the lipid monolayer at the air/buffer interface in the presence and absence of NPs. The lateral resolution of the microscope was 10 μm. All experiments were performed at ambient temperature (T=23±1 ºC).

2.5. Cell culture

RBE4 cells (a generous gift from Dr. Aschner, Vanderbilt University) were cultured on rat tail collagen type I (Millipore) at 37 °C and 5 % CO2 in 1:1 mixture of Minimum Essential Medium and Ham's F-10 medium supplemented with 10 % fetal bovine serum, 300 μg/ml geneticin and 1 ng/ml basic fibroblast growth factor (all from Thermo Scientific).

2.6. Flow cytometry

RBE4 cells were seeded on collagen type I in 12-well plates (Costar) at a density of 100,000 cells per well. When reaching the log phase, the cells were incubated with the NPs at 20 μg/ml in 1 ml of medium for 3 hours. After the cells were trypsinized and washed twice with phosphate-buffered saline (Sigma), they were analyzed by flow cytometry (Gallios, Beckman Coulter). NR668-loaded NPs were excited at 561 nm and fluorescence was detected at 620 nm using a 30 nm bandpass filter. p-HTAH-loaded NPs were excited at 405 nm and fluorescence was detected at 450 nm using a 50 nm bandpass filter. 10,000 cells were use in the analysis; cell debris, dead cells and aggregates were excluded by gating the cell population on a dot plot of forward light scatter signal versus side scatter signal. The cellular association and uptake of NPs was measured as the percentage of positive cells in flow cytometry histograms, and the amount of NPs per cell was estimated using median fluorescence intensity. To compare the cellular association and uptake of NPs which had different amount of encapsulated dye and, therefore, different fluorescence intensities, a normalization factor was used. This factor was found by measuring the fluorescence intensity of NPs in PBS using a spectrophotometer (Infinite 200Pro, Tecan) and was in the range of 1.0-2.9 depending on the NP.

2.7. Confocal laser scanning microscopy

The cells were seeded on collagen type I in 8-well Ibidi plates (Ibidi) at a density of 20,000 cells per well and grown to reach the log-phase. Following that, the cells were incubated with the NPs at 20 μg/ml in 250 μl of medium for 3 hours, then fixed in 4% paraformaldehyde and counter-stained with Hoechst 33258 (Life Technologies) to visualize the nuclei and Alexa Fluor 488-labeled phalloidin (Life Technologies) to visualize the actin cytoskeleton. After staining, the cells were prepared for imaging by mounting using SlowFade Gold Antifade Mountant (Life

Technologies). Confocal images were obtained using a Leica SP8 CLSM with a 63 × 1.2 water objective. For NR668 excitation, a white light laser at 514 nm was used, and the emission was detected at 580–660 nm using a photon counting hybrid detection system. For p-HTAH excitation, a 405 nm laser was used, and the emission was detected at 450-480 nm. Z-stacks of cells were obtained to distinguish between intracellular and surface-associated NPs.

2.8. Data analysis

Data on lipid monolayers were analyzed using Origin 8.1 software (OriginLab). Confocal images were analyzed using ImageJ. 1.48g. Flow cytometry data were analyzed using Kaluza Flow Cytometry Analysis software v1.2 (Beckman Coulter). Statistical analysis was performed using SPSS Statistics v20 (IBM).

3. Results

3.1. Nanoparticle composition and characterization

NPs with varying composition (type of PEG and monomer) were synthetized by miniemulsion polymerization and characterized with regard to size, charge and PEG density. NP composition, size and ζ-potential are given in Table 1.

Table 1. Composition and characterization of the NPs used in this study

Nanoparticles	Monomer	Size, nm	PDI	ζ-potential, mV	Initiator	Stabilizer	Dye	Ethylene glycol units/nm^2
B_Kol_Brij_1	BCA	117	0.11	-3	Kolliphor HS 15	Brij L23		14.8

B_Kol_Brij_1 *	BCA	145	0.24	-3	Kolliphor HS 15	Brij L23	NR668	20.0
IH_Kol_Brij_ 1	IHCA	143	0.13	-1	Kolliphor HS 15	Brij L23		27.9
IH_Kol_Brij_ 1*	IHCA	172	0.25	-2	Kolliphor HS 15	Brij L23	NR668	24.1
IH_Kol_Brij_ 2	IHCA	163	0.15	-1	Kolliphor HS 15	Brij L23	NR668	25.1
B_Jeff_Brij_1	BCA	103	0.26	-4	Jeffamine M-2070	Brij L23		17.4
B_Jeff_Brij_2	BCA	150	0.18	-2	Jeffamine M-2070	Brij L23	DiR	12.7
B_Jeff_Brij_3	BCA	158	0.32	-4	Jeffamine M-2070	Brij L23		19.8
B_Jeff_Brij_4	BCA	118	0.26	-3	Jeffamine M-2070	Brij L23	pHTAH	17.5
IH_Jeff_Brij_ 1	IHCA	169	0.21	-2	Jeffamine M-2070	Brij L23	NR668	21.9
IH_Jeff_Brij_ 2	IHCA	148	0.19	-3	Jeffamine M-2070	Brij L23		22.3
B_Kol_Plu_1	BCA	141	0.11	-5	Kolliphor HS 15	Pluronic F68		13.0
B_Kol_Plu_2	BCA	151	0.11	-5	Kolliphor HS 15	Pluronic F68	NR668	14.0
IH_Kol_Plu_1	IHCA	167	0.34	-2	Kolliphor HS 15	Pluronic F68		26.5

Throughout the text, the following conventions are used to describe the NPs for the sake of brevity: first, the monomer type (B or IH, denoting BCA and IHCA, respectively), followed by PEG type where Kol refers to Kolliphor, Jeff – to Jeffamine M-2070 and Brij – to Brij L23, and, ultimately, the number, in order to distinguish between NPs that share both the same monomer and a particular combination of PEG. It should be noted that B_Kol_Brij_1 and IH_Kol_Brij_1 were produced in two variants, with or without a fluorescent dye. This is reflected in the text below and discussed in more detail in the Discussion.

All NPs were within a relatively narrow size distribution (diameter 103-169 nm) and had a slightly negative charge (- 1 to -5 mV). In addition to the NP coating, ζ-potential depends on pH and ionic strength of the electrolyte. The value of ζ-potential is measured at the slip plane at the distance of approx. 2.5 nm from the Stern layer (for 10 mM NaCl solution) [31, 32]. In our case, the particle surface below the PEG layer is assumed to be a partly hydrolyzed polymer, therefore

negatively charged. The surface potential at this plane can be estimated by measurement of the ζ-potential of similar NPs with a very low PEG density, which is typically around -15 mV. Using PEG-based amphiphilic molecules as both stabilizers and initiators resulted in PEGylated particles with PEG density values in the range 14-28 ethylene glycol units per nm^2, with PEG covalently linked to the particle surface. This PEG density is obtained using access of PEG and removing non-reacted and unbound PEG by dialysis. The proposed surface functionalization of the three different PEGylation strategies used is illustrated in Supplementary Figure 1. Briefly, four different PEG-based surfactants were used to form three different PEG coating combinations. A: Brij L23 + Kolliphor HS15; B: Brij L23 + Jeffamine M2070 and C: Pluronic F68 + Kolliphor HS15.

3.2. Nanoparticle interaction with lipid monolayers

The kinetics of the interactions between the NPs and DMPC/DPPG monolayers modeling the cell membrane is shown in Supplementary Figure 2 for the initial surface pressure of π_0 = 20 mN/m. The addition of NPs induced an increase in the surface pressure, and the effect the NPs exerted on the monolayers is expressed in the changes in monolayer surface pressure $\Delta\pi$.

Such measurements were done for a variety of NPs, and NP-monolayer interaction is presentedin Figure 1 based on the magnitude of the surface pressure change. The cumulative changes in $\Delta\pi$ for different NPs (reached at the NP concentration of 80 μg/ml) are shown as well. These changes varied in the range of $\Delta\pi$ = 5-11 mN/m.

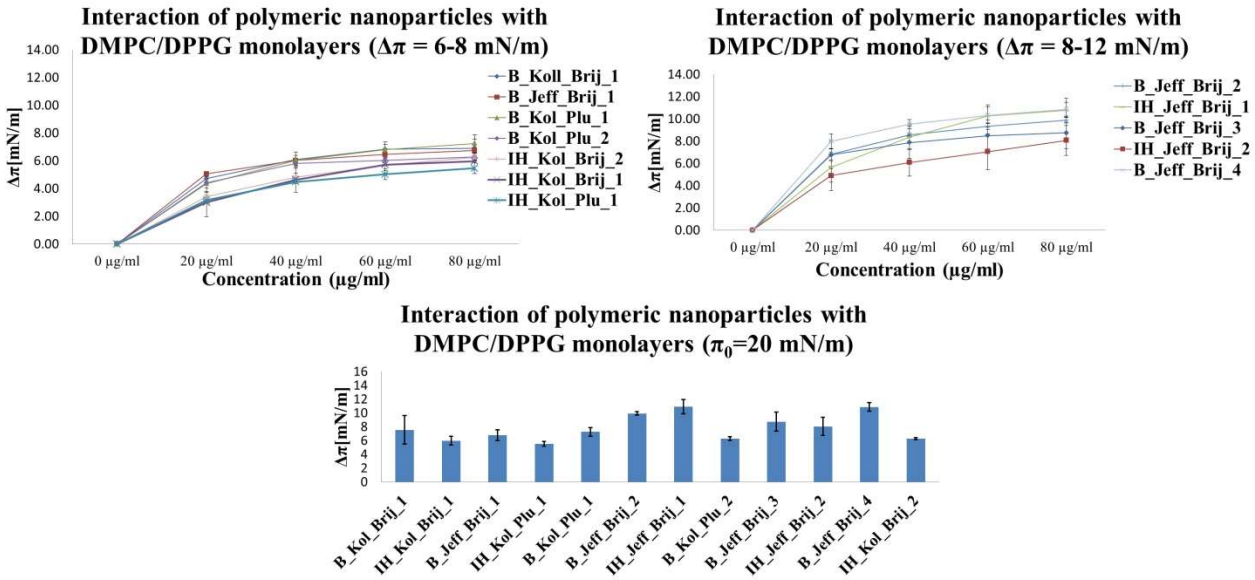

Figure 1. The plot of the changes in surface pressure vs. concentration of NPs following the interaction of PACA NPs with DMPC/DPPG monolayers at the initial surface pressure of π_0=20 mN/m. n=3-4. Interactions with a magnitude of Δπ reaching 5-8 and 8-11 mN/m, are shown in the left and right panel, respectively. Cumulative Δπ at the NP concentration of 80 µg/ml at the end of the experiment are shown as well.

Next we looked at the patterns of NP-monolayer interactions that could identify their correlation with various NP properties. Dependence of the cumulative surface pressure changes induced by NP-monolayer interactions on the PEG type, NP monomer type, PEG density, size and surface charge is shown in Figure 2.

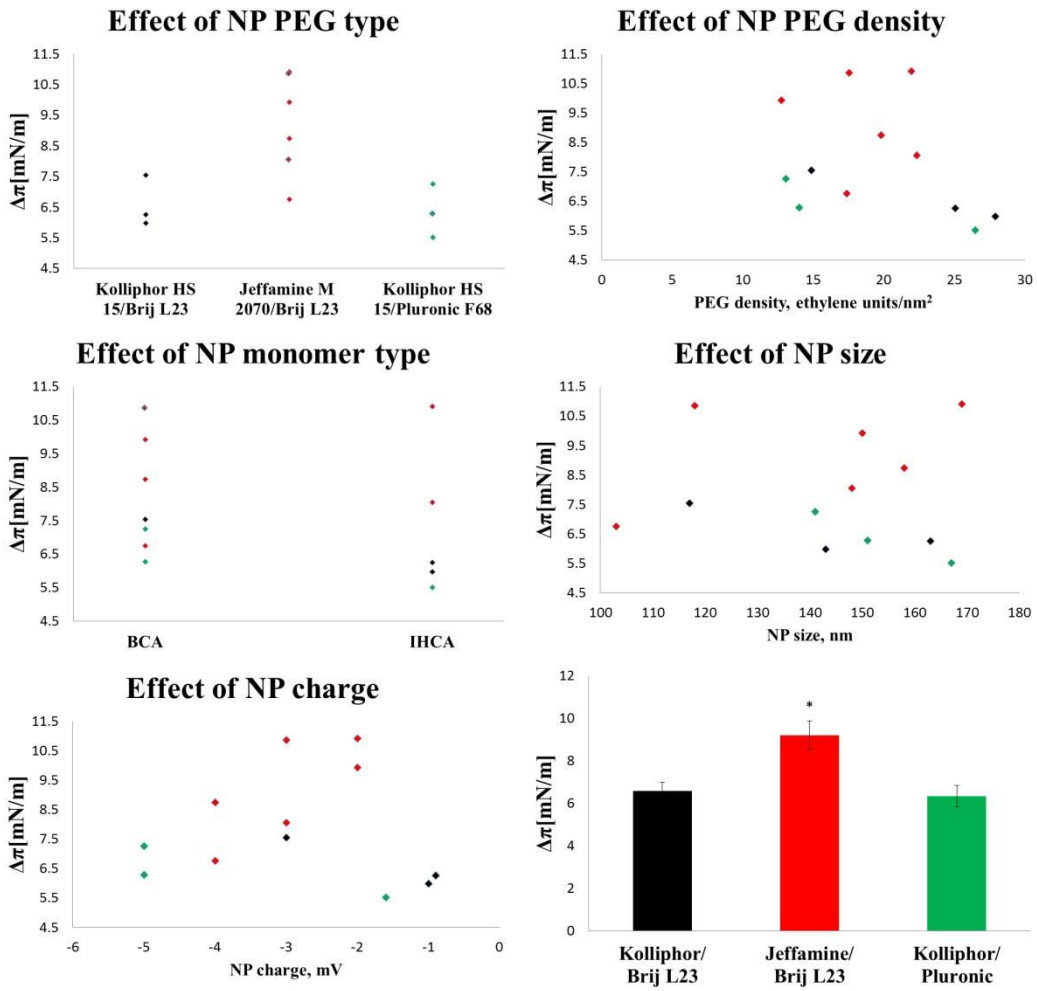

Figure 2. The effect of NP properties on the cumulative change in monolayer surface pressure change reached at the NP concentration of 80 µg/ml. Figure shows the effect of NP PEG type, PEG density, monomer type, NP diameter and NP surface charge. Black diamonds: Koliphor HS 15/Brij L23; red diamonds: Jeffamine M 2070/Brij L23; green diamonds: Koliphor HS 15/Pluronic F68. Changes in the cumulative surface pressure for PACA NPs having the same PEG combination and interacting with DMPC/DPPG monolayers at π_0=20 mN/m are shown as well. n=3-15 depending on the group. Asterisk denotes statistically significant difference ($p<0.05$) according to Mann-Whitney U test.

NP monomer type did not have any statistically significant effect on the strength of NP-monolayer interactions in the Mann-Whitney U test. PEG density, NP size and NP surface charge did not correlate with the effect that PACA NPs exerted on lipid monolayers either (R^2=0.11, R^2<0.1 and R^2<0.1, respectively, according to linear regression analysis). With respect to the last three properties, this can be attributed to their relatively narrow distribution in the NPs used. However, various PEG type combinations induced markedly different changes in the monolayer surface pressure. Except for one outlier (B_Jeff_Brij_1), all NPs having the PEG combination Jeffamine M2070/Brij L23 induced surface pressure changes ($\Delta\pi$ = 8.74-10.91 mN/m) well above the other NPs which caused cumulative surface pressure changes in the range of $\Delta\pi$ = 5.51-7.54 mN/m. To emphasize this, data points in Figure 2 were color-coded according to the PEGylation type. Further illustration of this point is also provided in Figure 2 where cumulative surface pressure changes induced by NPs were averaged for all NPs with the same PEG type. This shows that the effect of PACA NPs with Jeffamine M 2070/Brij L23 is significantly larger than the effect produced by NPs with other PEG combinations.

In order to visualize interactions between polymeric NPs and DMPC/DPPG monolayers, we chose NPs producing the largest cumulative effect on the monolayer surface pressure and monitored its interactions with the monolayer using Brewster angle microscopy (Figure 3).

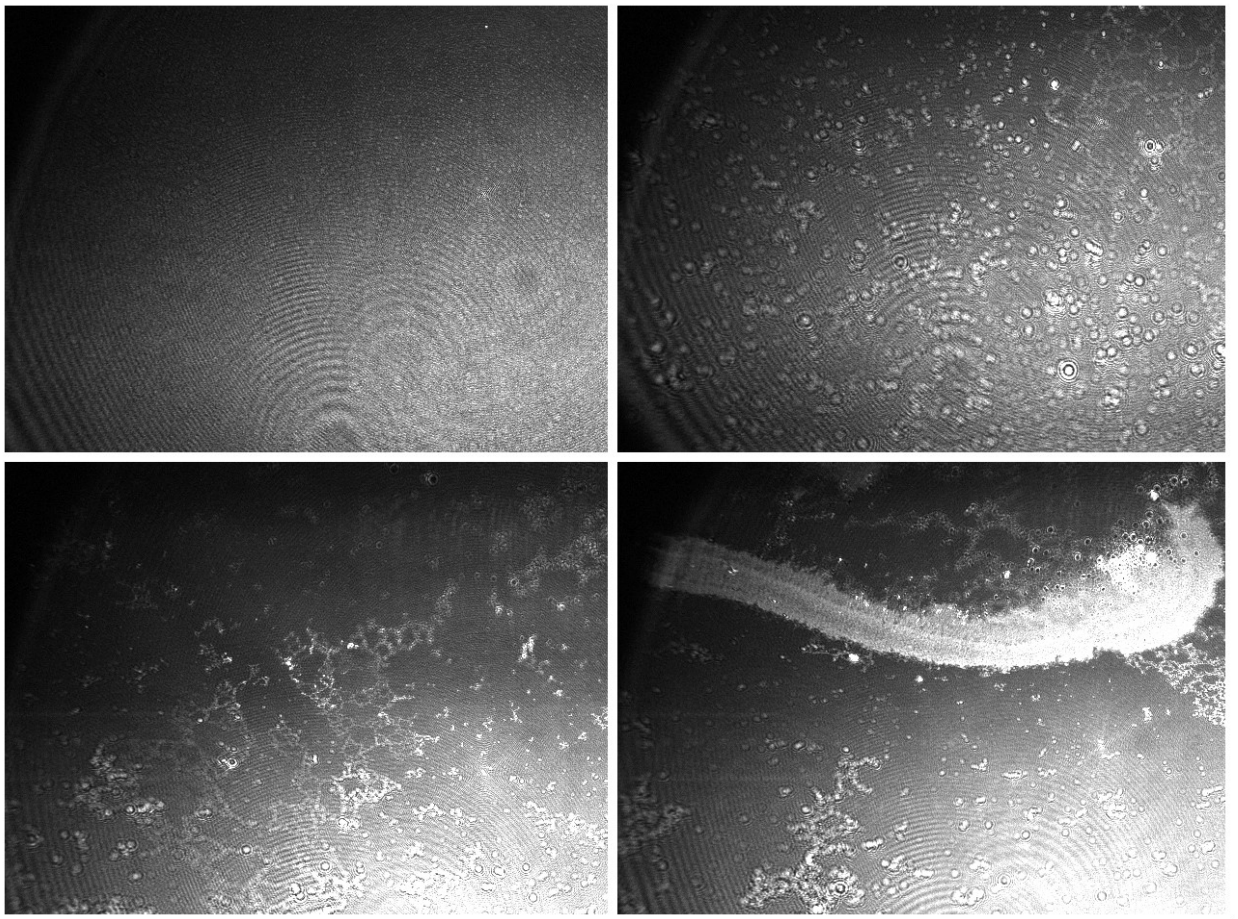

Figure 3. Visualization of interaction between B_Jeff_Brij_4 and DMPC/DPPG monolayer at π_0=20 mN/m. Figure shows the monolayer before the addition of NPs and progressive formation of NP-induced lipid clustering after the addition of B_Jeff_Brij_4 NPs at 20, 60 and 80 µg/ml, respectively.

The effect of B_Jeff_Brij_4 NPs can be seen in in the formation of increasingly denser bright clusters caused by the interaction of the NPs with the monolayer. A recording showing real-time monitoring of NP interactions with a DMPC/DPPG monolayer is shown in Supplementary Video 1.

While most of the monolayer interaction results were produced by measuring NP interactions with the DMPC/DPPG monolayer at an initial surface pressure of 20 mN/m, in separate experiments we found that the extent of the effect depended on the initial surface pressure π_0. At the initial surface pressure values of 10 and 30 mN/m, surface pressure changes induced by NPs with the PEG combination producing the largest effect (B_Jeff_Brij_4) were found to be larger and smaller than the values reached at π_0 = 20 mN/m, respectively (Supplementary Figures S3-S4). Additionally, we investigated whether the presence or absence of a fluorescent dye in B_Kol_Brij_1 could cause any changes in NP-monolayer interactions. Both types of B_Kol_Brij_1 caused similar changes in the surface pressure of the lipid monolayers (Supplementary Figure S5).

3.3. Cellular association and uptake

In order to investigate whether the cellular association and uptake of the NPs by living cells are affected by NP properties and compare that to the effect of the NPs on lipid monolayers, we incubated RBE4 cells with the NPs for 3 hours and measured fluorescence of the cell populations using flow cytometry. Since detection of cell surface-associated or internalized NPs by flow cytometry relies on their fluorescence, we could only use NPs labeled with a fluorescent dye. In the case of B_Kol_Brij_1 and IH_Kol_Brij_1 (all labeled with NR668), the NPs were originally made in two variants: with and without a fluorescent dye. Representative flow cytometry histograms illustrating low and high cellular fluorescence intensities, as well as the median fluorescence intensity for all NPs studied, corrected for the difference in fluorescence intensities, are shown in Figure 4.

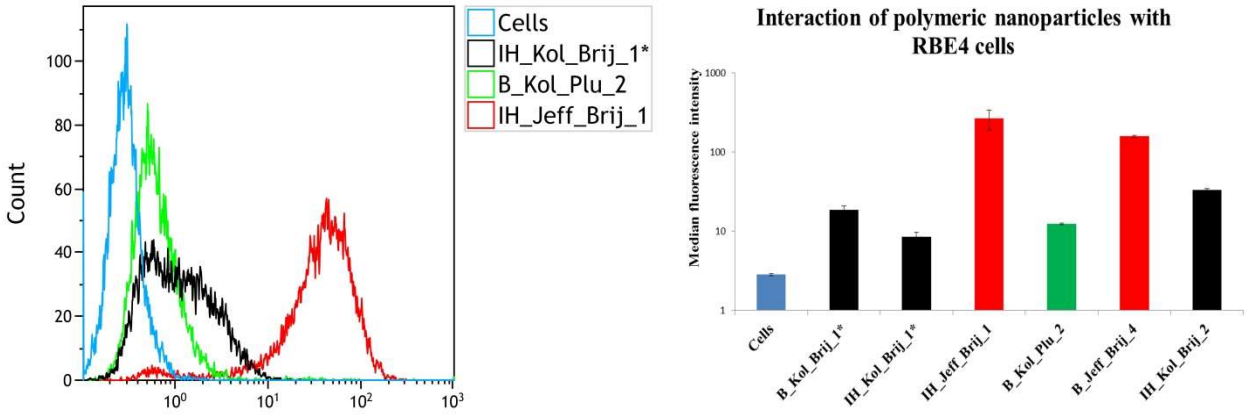

Figure 4. Cell surface association and uptake of polymeric NPs by RBE4 cells showing representative flow cytometry histograms and median fluorescence intensities of cells incubated with the NPs and corrected for variations in fluorescence intensities.

The fluorescence of RBE4 cells incubated with NPs for 3 hours was mainly limited, with the exceptions of two NPs: IH_Jeff_Brij_1 and B_Jeff_Brij_4. It should be noted that both of these NPs also had the largest effect on DMPC/DPPG monolayer surface pressure in the lipid monolayer experiments. In order to detect any dependence between NP properties and cellular association/uptake, we plotted the changes in fluorescence intensity induced by cellular association and uptake against the various NPs properties (Figure 5).

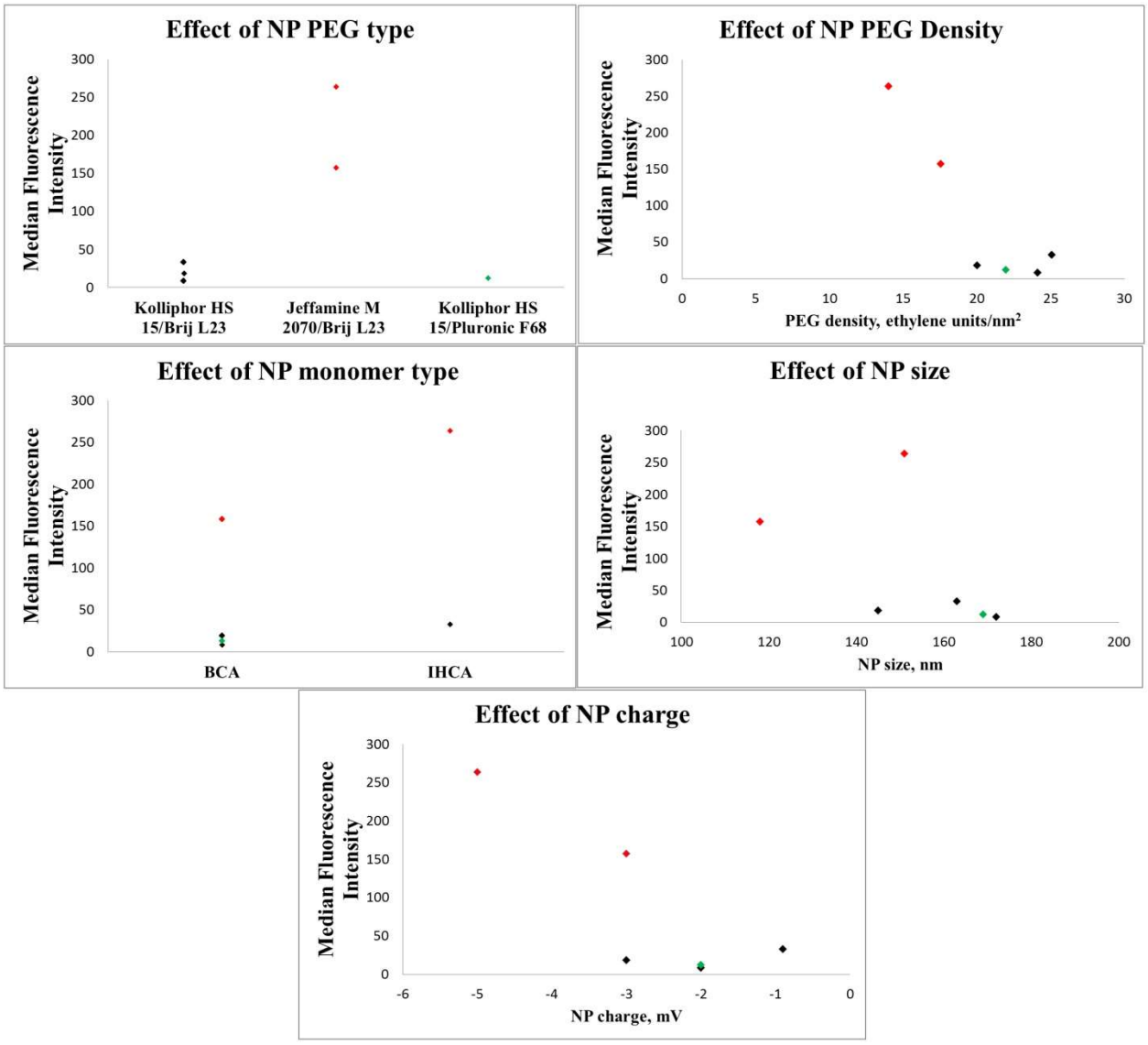

Figure 5. The effect of NP properties on the cellular association and uptake of NPs by RBE4 cells. Figure shows the effect of NP PEG type, PEG density, monomer type, NP size and NP surface charge. Black diamonds: Koliphor HS 15/Brij L23; red diamonds: Jeffamine M 2070/Brij L23; green diamonds: Koliphor HS 15/Pluronic F68.

Figure 5 shows that the type of PEG and PEG density affected NP uptake by cells or their association with the plasma membrane. Increased PEG density resulted in reduced cellular

association and uptake (R^2=0.80 according to linear regression analysis), an observation in line with the literature [10]. However, this did not translate into reduced interaction with lipid monolayers regardless of whether linear regression analysis included all NPs in the lipid monolayer studies (R^2=0.11) or only those that were also used in cellular association and uptake studies (R^2=0.04). NP size and charge were not strongly correlated with NP cellular uptake either (R^2=0.27 and 0.69, respectively). One result that was clear both in the cellular studies and in PACA NP interactions with lipid monolayers was the effect of the PEG type. Both NPs that showed the highest association with and uptake by RBE4 cells were PEGylated using Jeffamine M-2070 as the initiator and Brij L23 as the stabilizer. As in Figure 2, data points in Figure 5 were color-coded to emphasize this observation.

Flow cytometry cannot distinguish between surface-associated and internalized NPs, and since the dyes in our particles are encapsulated rather than bound to the surface of the NPs, quenching them with traditional quenching agents such as Trypan Blue may be problematic due to the increased distance between the dyes and the quencher. We therefore acquired confocal images of RBE4 cells incubated with the polymeric NPs, taking Z-stacks in order to verify the intracellular location of the NPs (Figure 6).

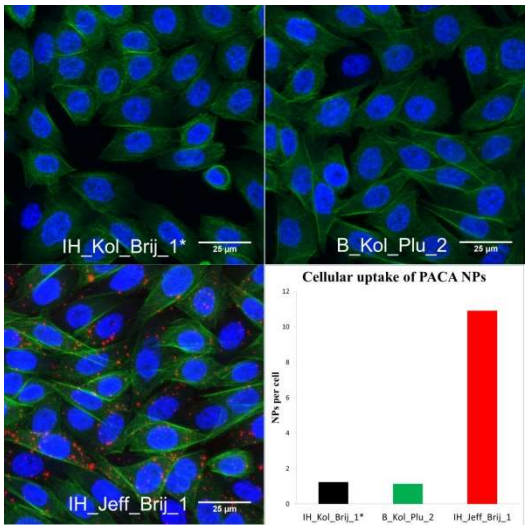

Figure 6. Uptake of NPs by RBE4 cells. Confocal images of the uptake of various NPs by RBE4 cells shown with quantification of NP uptake using image analysis to count the number of NPs per cell. Blue: cell nuclei, green: actin filaments, red: NPs; maximum intensity projections.

Confocal microscopy images are consistent with the flow cytometry data. In Figure 6, the uptake of IH_Jeff_Brij_1 NPs appears to be far greater than that of the other NPs. Visual inspection is supported by image analysis estimating the number of NPs per cell.

Finally, we analyzed the correlation between surface pressure changes induced by PACA NPs and the extent of their cellular uptake (Figure 7).

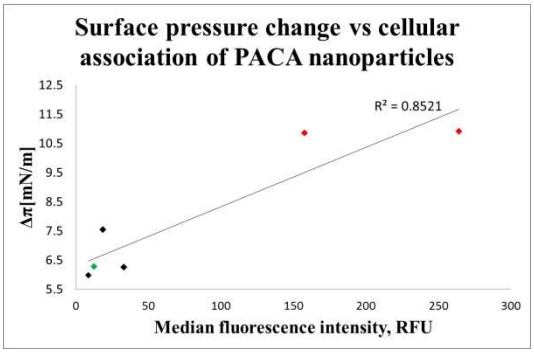

Figure 7. Correlation between PACA NP effects on lipid monolayers and their cellular association and uptake.

Figure 7 clearly shows a correlation between changes in surface pressure and cellular uptake, i.e. the PACA NPs that had the largest effect in monolayer studies also exhibited the highest cellular uptake.

4. Discussion

The interactions between NPs and cells are initiated at the cell membrane. Therefore, understanding how these interactions are affected by various NP properties is crucial for designing NPs for drug delivery. The interactions may be probed in a variety of cell membrane models including lipid monolayers, liposomes and supported lipid bilayers. Our study with lipid monolayers shows that the addition of NPs into the water subphase resulted in increased surface pressure depending on the type of NP coating. This is evidence of interactions between NPs with phospholipid head groups of the monolayer. The adsorption of charged NPs results in increasing repulsive forces in the monolayers, which is the main reason of the surface pressure changes. Surface pressure changes therefore can be used to assess the extent of the effect that the NPs exert on the lipid monolayer. The surface pressure depends on the mean molecular area and reflects the spacing of lipid molecules in the monolayer. High surface pressure and low molecular area indicate that the lipid molecules are closely packed, and vice versa [23]. Changes in the surface pressure can be induced by interaction with foreign agents such as PACA NPs in this study. Different surface pressure values can be used to model normal cells (30 mN/m) and cancer cells (20 mN/m)

which have varying lipid densities in the outer cell membrane. At the same time, NP charge had no significant effect on the interaction with negatively charged monolayers. The interaction between NPs and the lipid membrane depends on the charge of both NPs and the lipid film. A detailed theoretical and experimental study has been recently performed by Velikonja et al [33] and Santosh et al [34]. They showed that interaction of negatively charged NPs with negatively charged vesicles is restricted due to repulsive forces, while interaction between these NPs with zwitterionic lipids is favorable due to positively charged choline groups. The dipole moments of the polar head groups are in this case oriented more perpendicularly to the membrane surface [33]. The results obtained in our work are in good agreement with the above-mentioned papers. The ζ-potential of the liposomes composed of the mixture of DMPC/DPPG (molar ratio 10:1) determined in our recent work is approx. -30 mV [22]. Therefore, the monolayers composed of this mixture are also negatively charged owing to the presence of negatively charged DPPG. However, due to the presence of DMPC, a zwitterionic lipid, the interaction between negatively charged NPs and the monolayers can be described as interplay between repulsive and attractive forces. For most of the NPs, we did not observe a correlation between NP charge and changes in surface pressure. The only exception is NPs with Jeffamine M-2070/Brij L23 PEG coating (see Fig. 2), for which a certain decrease in surface pressure was observed with increasing negative charge of NPs. This suggests that this interaction is determined by repulsive forces between negatively charged NPs and negatively charged monolayer. However, for other NPs, we did not observe this correlation. This may be linked to the lack of correlation between NPs charge and PEG surface density as well as to the rather narrow variation of the negative charge of NPs. Changes in the ζ-potential of NPs in this rather narrow range should not have affected interaction with negatively charged monolayer surface composed of DMPC/DMPPG mixture. Even though the DMPC fraction is dominant in the

mixed monolayers, the presence of negatively charged DPPG head groups should result in the tilting of dipoles in zwitterionic lipids in the direction parallel to the monolayer surface. This effect should further enhance repulsive forces between NPs and monolayer surface. The effect of NP size and charge on the cellular uptake has been demonstrated in numerous works [35, 36], and the general trends seem to be valid for interactions between NPs and model membranes as well. In [23], relatively small polystyrene NPs (20 nm) increased the surface pressure of a model endothelial membrane regardless of surface chemistry, while larger NPs (≥60 nm) either reduced it or had no effect, depending on the surface group. At a size of 60 nm, aminated NPs increased the surface pressure of the endothelial monolayer model, while unmodified NPs reduced it and carboxylated NPs had no effect. In our study, PACA NPs were rather large and in a narrow size range of 103-167 nm and the size did not have any effect on the magnitude of NP-monolayer or NP-cell interactions. The discrepancy between our results and the results in the study referred to might be due to the different type or size of the NPs.

NPs used as drug carriers are commonly coated or otherwise functionalized to ensure specific drug delivery. Such coatings and functional groups are on the external surface of the NP and, therefore, are the first moieties recognized by the plasma membrane. Consequently, their interactions with the cell membrane largely define the outcome of NP-cell interaction. The effect of cationic surfactants on the interactions between PLGA NPs of approximately the same size and model plasma and endosome membranes [19] indicated that cationic PLGA NPs coated with didodecyldimethylammonium bromide (DMAB) or cetyltrimethylammonium bromide (CTAB) increased the surface pressure of the model membranes as opposed to unmodified anionic NPs, and that the increase induced by DMAB NPs was faster and larger than that caused by CTAB NPs. Cellular uptake studies were in line with monolayer experiments. The same group demonstrated

that neither ritonavir-loaded poly(l-lactide) NPs (RNPs), nor RNPs conjugated to a scrambled trans-activating transcriptor peptide had an effect on a lipid monolayer mimicking an endothelial cell membrane, while RNPs conjugated to the actual peptide affected the membrane depending on the amount of the peptide on the RNPs; cellular studies using human vascular endothelial cells showed good correlation with lipid monolayer experiments [20].

NP PEGylation is among the most common methods to avoid NP interception by the RES in vivo. It can also reduce the toxicity of nanoparticles [37], although both effects can come at the expense of reduced interaction with and uptake by cells. Among factors that affect the balance between efficient shielding from the RES and uptake by target cells are PEG molecular weight, chain structure, conformation and coating density. PEG chain length, in particular, has been shown to affect cell binding and uptake of several NP platforms [38, 39]. It has also been noted, however, that the evaluation of PEGylation efficiency suffers from a large variability of results across different NP platforms [40]. Our aim with regard to PEG properties was therefore to test a number of PEG combinations with short and long chains to determine if any of them facilitates NP-lipid monolayer and NP-cell interactions. Assuming that the chain length of each individual PEG component on the NP used in our study is given by the number of ethylene glycol units, our results indicate that the chain length is not an important parameter for the NP-monolayer interactions. However, such conclusions should be carefully considered as the actual PEG lengths on the NPs may change during synthesis and in solution. Therefore, each combination of PEG initiators and stabilizers used in our study is treated as a separate property without further assumptions concerning the length of individual components of the PEG coating.

While this study is the first to probe the effect of PEG type on PACA NP interactions with model membranes, the interactions of various polymers with cell membrane models have been assessed

in several studies. With regard to PEG, a study comparing various Pluronic copolymers found that their effect on drug efflux activity in brain endothelial cells and cancer cells depended on molecule hydrophobicity and the lengths of the hydrophobic and hydrophilic segments [41]. A subsequent study found that not only the overall hydrophobicity, but also the structure of PEG copolymers affected their interactions with lipid bilayers [42]. It should be noted that both the membrane model itself and the readouts were markedly different from the ones used in the present study. The effects of various Pluronics on lipid monolayer surface pressure [43] showed that Pluronics with higher hydrophobicities exerted greater effects on DMPC and DPPC monolayers. In yet another study, it was found that the size of Pluronic molecules governed their insertion in DPPC and DPPG monolayers, with smaller molecules being able to insert into monolayers at higher surface pressure than larger ones [44]. It should be emphasized that in our study, the external agents interacting with the DMPC/DPPG monolayer were PACA NPs coated with PEG, as opposed to surfactant molecules alone; however, since the size distribution of the NPs remained relatively narrow, the structure and relative sizes of the copolymer blocks may have played a dominant role in the interaction.

We should note that the encapsulation of dyes into NPs can cause misinterpretation of their cellular uptake in flow cytometry due to potential dye leakage [45-47]. We therefore confirmed that no dye leakage has taken place by incubating RBE4 cells with PACA NPs at 4 ºC [48]. In addition, CLSM images confirmed that the NPs were internalized.

Various properties of NPs, particularly the size and charge that most NP platform are normally characterized for, have been shown to affect NP cellular uptake to some extent; however, as noted by [49, 50], those properties can hardly be used as reliable predictors, and NP interactions with

model cell membranes having properties typical for target cells may be employed to assess NP cellular uptake potential with greater precision [23].

In conclusion, this is to the best of our knowledge the first study investigating the interactions between PACA NPs and a model cell membrane and correlating these interactions with NP cellular uptake, with particular emphasis on PACA NP monomer type and PEGylation. We observed a good correlation between PACA NPs interactions with a model membrane and their actual cellular uptake, and found that a particular combination of PEG altered NP effects in both systems. These results could be used in predicting PACA NP interactions with target cells and in designing PACA NP-based drug delivery systems with desired cellular uptake properties.

ACKNOWLEDGEMENTS:

Anne Rein Hatletveit, Zuzana Garaiova, Pavol Vitovič, Július Cirák, Juraj Chlpík and Tomas Vary are thanked for technical assistance with nanoparticle synthesis, Langmuir-Blodgett troughs and Brewster angle microscopy experiments. This study was funded by The Central Norway Regional Health Authority and The Research Council of Norway (NANO2021 project number 220005 and BIOTEK2021 project number 226159), as well as the Stipend program EEA Slovakia - institutional collaboration between high education institutions EEA/EHP-SK06-IV-V-01 (project No. SK06-IV-01-005), Agency for Promotion Research and Development under the contract APVV-14-0267 and Science Grant Agency VEGA (project No. 1/0152/15).

REFERENCES:

[1] N. Bertrand, J. Wu, X. Xu, N. Kamaly, O.C. Farokhzad, Cancer nanotechnology: the impact of passive and active targeting in the era of modern cancer biology, Advanced drug delivery reviews, 66 (2014) 2-25.
[2] J.L. Markman, A. Rekechenetskiy, E. Holler, J.Y. Ljubimova, Nanomedicine therapeutic approaches to overcome cancer drug resistance, Advanced drug delivery reviews, 65 (2013) 1866-1879.
[3] E.H. Chang, J.B. Harford, M.A. Eaton, P.M. Boisseau, A. Dube, R. Hayeshi, H. Swai, D.S. Lee, Nanomedicine: Past, present and future - A global perspective, Biochemical and biophysical research communications, 468 (2015) 511-517.
[4] B.D. Chithrani, A.A. Ghazani, W.C. Chan, Determining the size and shape dependence of gold nanoparticle uptake into mammalian cells, Nano letters, 6 (2006) 662-668.
[5] C. He, Y. Hu, L. Yin, C. Tang, C. Yin, Effects of particle size and surface charge on cellular uptake and biodistribution of polymeric nanoparticles, Biomaterials, 31 (2010) 3657-3666.
[6] R. Ferrari, M. Lupi, C. Colombo, M. Morbidelli, M. D'Incalci, D. Moscatelli, Investigation of size, surface charge, PEGylation degree and concentration on the cellular uptake of polymer nanoparticles, Colloids and surfaces. B, Biointerfaces, 123 (2014) 639-647.
[7] Y. Li, M. Kroger, W.K. Liu, Shape effect in cellular uptake of PEGylated nanoparticles: comparison between sphere, rod, cube and disk, Nanoscale, 7 (2015) 16631-16646.
[8] D.F. Moyano, K. Saha, G. Prakash, B. Yan, H. Kong, M. Yazdani, V.M. Rotello, Fabrication of corona-free nanoparticles with tunable hydrophobicity, ACS nano, 8 (2014) 6748-6755.
[9] M.J. Ernsting, M. Murakami, A. Roy, S.D. Li, Factors controlling the pharmacokinetics, biodistribution and intratumoral penetration of nanoparticles, Journal of controlled release : official journal of the Controlled Release Society, 172 (2013) 782-794.
[10] S.J. Soenen, B.B. Manshian, A.M. Abdelmonem, J.-M. Montenegro, S. Tan, L. Balcaen, F. Vanhaecke, A.R. Brisson, W.J. Parak, S.C. De Smedt, K. Braeckmans, The Cellular Interactions of PEGylated Gold Nanoparticles: Effect of PEGylation on Cellular Uptake and Cytotoxicity, Particle & Particle Systems Characterization, 31 (2014) 794-800.
[11] D. Pozzi, V. Colapicchioni, G. Caracciolo, S. Piovesana, A.L. Capriotti, S. Palchetti, S. De Grossi, A. Riccioli, H. Amenitsch, A. Lagana, Effect of polyethyleneglycol (PEG) chain length on the bio-nano-interactions between PEGylated lipid nanoparticles and biological fluids: from nanostructure to uptake in cancer cells, Nanoscale, 6 (2014) 2782-2792.
[12] A. Kumari, S.K. Yadav, S.C. Yadav, Biodegradable polymeric nanoparticles based drug delivery systems, Colloids and surfaces. B, Biointerfaces, 75 (2010) 1-18.
[13] E. Soma*, P. Attali, P. Merle, Chapter 11 A Clinically Relevant Case Study: the Development of Livatag[registered sign] for the Treatment of Advanced Hepatocellular Carcinoma, Nanostructured Biomaterials for Overcoming Biological Barriers, The Royal Society of Chemistry2012, pp. 591-600.
[14] C. Vauthier, D. Labarre, G. Ponchel, Design aspects of poly(alkylcyanoacrylate) nanoparticles for drug delivery, Journal of drug targeting, 15 (2007) 641-663.
[15] L. Treuel, X. Jiang, G.U. Nienhaus, New views on cellular uptake and trafficking of manufactured nanoparticles, Journal of the Royal Society, Interface / the Royal Society, 10 (2013) 20120939.
[16] E. Rascol, J.M. Devoisselle, J. Chopineau, The relevance of membrane models to understand nanoparticles-cell membrane interactions, Nanoscale, 8 (2016) 4780-4798.
[17] C. Stefaniu, G. Brezesinski, H. Möhwald, Langmuir monolayers as models to study processes at membrane surfaces, Advances in Colloid and Interface Science, 208 (2014) 197-213.
[18] A.A. Torrano, A.S. Pereira, O.N. Oliveira, Jr., A. Barros-Timmons, Probing the interaction of oppositely charged gold nanoparticles with DPPG and DPPC Langmuir monolayers as cell membrane models, Colloids and surfaces. B, Biointerfaces, 108 (2013) 120-126.

[19] C. Peetla, V. Labhasetwar, Effect of molecular structure of cationic surfactants on biophysical interactions of surfactant-modified nanoparticles with a model membrane and cellular uptake, Langmuir : the ACS journal of surfaces and colloids, 25 (2009) 2369-2377.
[20] C. Peetla, K.S. Rao, V. Labhasetwar, Relevance of biophysical interactions of nanoparticles with a model membrane in predicting cellular uptake: study with TAT peptide-conjugated nanoparticles, Molecular pharmaceutics, 6 (2009) 1311-1320.
[21] A. Ambike, V. Rosilio, B. Stella, S. Lepetre-Mouelhi, P. Couvreur, Interaction of self-assembled squalenoyl gemcitabine nanoparticles with phospholipid-cholesterol monolayers mimicking a biomembrane, Langmuir : the ACS journal of surfaces and colloids, 27 (2011) 4891-4899.
[22] M. Ionov, K. Ciepluch, Z. Garaiova, S. Melikishvili, S. Michlewska, L. Balcerzak, S. Glinska, K. Milowska, R. Gomez-Ramirez, F.J. de la Mata, D. Shcharbin, I. Waczulikova, M. Bryszewska, T. Hianik, Dendrimers complexed with HIV-1 peptides interact with liposomes and lipid monolayers, Biochimica et biophysica acta, 1848 (2015) 907-915.
[23] C. Peetla, V. Labhasetwar, Biophysical characterization of nanoparticle-endothelial model cell membrane interactions, Molecular pharmaceutics, 5 (2008) 418-429.
[24] E. Sulheim, H. Baghirov, E. von Haartman, A. Boe, A.K. Aslund, Y. Morch, L. Davies Cde, Cellular uptake and intracellular degradation of poly(alkyl cyanoacrylate) nanoparticles, Journal of nanobiotechnology, 14 (2016) 1.
[25] C. Lherm, R.H. Müller, F. Puisieux, P. Couvreur, Alkylcyanoacrylate drug carriers: II. Cytotoxicity of cyanoacrylate nanoparticles with different alkyl chain length, International Journal of Pharmaceutics, 84 (1992) 13-22.
[26] Y. Morch, R. Hansen, S. Berg, A.K. Aslund, W.R. Glomm, S. Eggen, R. Schmid, H. Johnsen, S. Kubowicz, S. Snipstad, E. Sulheim, S. Hak, G. Singh, B.H. McDonagh, H. Blom, C. de Lange Davies, P.M. Stenstad, Nanoparticle-stabilized microbubbles for multimodal imaging and drug delivery, Contrast media & molecular imaging, 10 (2015) 356-366.
[27] A.S. Klymchenko, E. Roger, N. Anton, H. Anton, I. Shulov, J. Vermot, Y. Mely, T.F. Vandamme, Highly lipophilic fluorescent dyes in nano-emulsions: towards bright non-leaking nano-droplets, RSC Advances, 2 (2012) 11876-11886.
[28] A. Aslund, C.J. Sigurdson, T. Klingstedt, S. Grathwohl, T. Bolmont, D.L. Dickstein, E. Glimsdal, S. Prokop, M. Lindgren, P. Konradsson, D.M. Holtzman, P.R. Hof, F.L. Heppner, S. Gandy, M. Jucker, A. Aguzzi, P. Hammarstrom, K.P. Nilsson, Novel pentameric thiophene derivatives for in vitro and in vivo optical imaging of a plethora of protein aggregates in cerebral amyloidoses, ACS chemical biology, 4 (2009) 673-684.
[29] Y. Zhang, M. Yang, N.G. Portney, D. Cui, G. Budak, E. Ozbay, M. Ozkan, C.S. Ozkan, Zeta potential: a surface electrical characteristic to probe the interaction of nanoparticles with normal and cancer human breast epithelial cells, Biomedical microdevices, 10 (2008) 321-328.
[30] O.V. Bondar, D.V. Saifullina, Shakhmaeva, II, Mavlyutova, II, T.I. Abdullin, Monitoring of the Zeta Potential of Human Cells upon Reduction in Their Viability and Interaction with Polymers, Acta naturae, 4 (2012) 78-81.
[31] M. Lorenzetti, E. Gongadze, M. Kulkarni, I. Junkar, A. Iglič, Electrokinetic Properties of TiO2 Nanotubular Surfaces, Nanoscale Research Letters, 11 (2016) 378.
[32] D.R. Woods, E. Diamadopolous, Importance of surfactants and surface phenomena on separating dilute oil-water emulsions and dispersions, Surfactants Chem/Process Eng, 19 (1988).
[33] A. Velikonja, P. Santhosh, E. Gongadze, M. Kulkarni, K. Eleršič, Š. Perutkova, V. Kralj-Iglič, N. Ulrih, A. Iglič, Interaction between Dipolar Lipid Headgroups and Charged Nanoparticles Mediated by Water Dipoles and Ions, International Journal of Molecular Sciences, 14 (2013) 15312.

[34] P.B. Santhosh, A. Velikonja, Š. Perutkova, E. Gongadze, M. Kulkarni, J. Genova, K. Eleršič, A. Iglič, V. Kralj-Iglič, N.P. Ulrih, Influence of nanoparticle–membrane electrostatic interactions on membrane fluidity and bending elasticity, Chemistry and Physics of Lipids, 178 (2014) 52-62.
[35] V. Mailander, K. Landfester, Interaction of nanoparticles with cells, Biomacromolecules, 10 (2009) 2379-2400.
[36] K. Kettler, K. Veltman, D. van de Meent, A. van Wezel, A.J. Hendriks, Cellular uptake of nanoparticles as determined by particle properties, experimental conditions, and cell type, Environmental Toxicology and Chemistry, 33 (2014) 481-492.
[37] M. Yu, S. Huang, K.J. Yu, A.M. Clyne, Dextran and polymer polyethylene glycol (PEG) coating reduce both 5 and 30 nm iron oxide nanoparticle cytotoxicity in 2D and 3D cell culture, Int J Mol Sci, 13 (2012) 5554-5570.
[38] L.J. Cruz, P.J. Tacken, R. Fokkink, C.G. Figdor, The influence of PEG chain length and targeting moiety on antibody-mediated delivery of nanoparticle vaccines to human dendritic cells, Biomaterials, 32 (2011) 6791-6803.
[39] R. Gref, M. Luck, P. Quellec, M. Marchand, E. Dellacherie, S. Harnisch, T. Blunk, R.H. Muller, 'Stealth' corona-core nanoparticles surface modified by polyethylene glycol (PEG): influences of the corona (PEG chain length and surface density) and of the core composition on phagocytic uptake and plasma protein adsorption, Colloids and surfaces. B, Biointerfaces, 18 (2000) 301-313.
[40] M.D. Howard, M. Jay, T.D. Dziubla, X. Lu, PEGylation of Nanocarrier Drug Delivery Systems: State of the Art, Journal of Biomedical Nanotechnology, 4 (2008) 133-148.
[41] E.V. Batrakova, S. Li, V.Y. Alakhov, D.W. Miller, A.V. Kabanov, Optimal structure requirements for pluronic block copolymers in modifying P-glycoprotein drug efflux transporter activity in bovine brain microvessel endothelial cells, The Journal of pharmacology and experimental therapeutics, 304 (2003) 845-854.
[42] T. Demina, I. Grozdova, O. Krylova, A. Zhirnov, V. Istratov, H. Frey, H. Kautz, N. Melik-Nubarov, Relationship between the Structure of Amphiphilic Copolymers and Their Ability To Disturb Lipid Bilayers, Biochemistry, 44 (2005) 4042-4054.
[43] L.C. Chang, C.Y. Lin, M.W. Kuo, C.S. Gau, Interactions of Pluronics with phospholipid monolayers at the air-water interface, Journal of colloid and interface science, 285 (2005) 640-652.
[44] S.A. Maskarinec, K.Y.C. Lee, Comparative Study of Poloxamer Insertion into Lipid Monolayers, Langmuir : the ACS journal of surfaces and colloids, 19 (2003) 1809-1815.
[45] S. Snipstad, S. Westrom, Y. Morch, M. Afadzi, A.K. Aslund, C. de Lange Davies, Contact-mediated intracellular delivery of hydrophobic drugs from polymeric nanoparticles, Cancer nanotechnology, 5 (2014) 8.
[46] T. Tenuta, M.P. Monopoli, J. Kim, A. Salvati, K.A. Dawson, P. Sandin, I. Lynch, Elution of labile fluorescent dye from nanoparticles during biological use, PloS one, 6 (2011) e25556.
[47] A. Salvati, C. Aberg, T. dos Santos, J. Varela, P. Pinto, I. Lynch, K.A. Dawson, Experimental and theoretical comparison of intracellular import of polymeric nanoparticles and small molecules: toward models of uptake kinetics, Nanomedicine : nanotechnology, biology, and medicine, 7 (2011) 818-826.
[48] S. Snipstad, S. Hak, H. Baghirov, E. Sulheim, Y. Morch, S. Lelu, E. von Haartman, M. Back, K.P. Nilsson, A.S. Klymchenko, C. de Lange Davies, A.K. Aslund, Labeling nanoparticles: Dye leakage and altered cellular uptake, Cytometry. Part A : the journal of the International Society for Analytical Cytology, (2016).
[49] J.L. Townson, Y.S. Lin, J.O. Agola, E.C. Carnes, H.S. Leong, J.D. Lewis, C.L. Haynes, C.J. Brinker, Re-examining the size/charge paradigm: differing in vivo characteristics of size- and charge-matched mesoporous silica nanoparticles, Journal of the American Chemical Society, 135 (2013) 16030-16033.
[50] L. Shang, K. Nienhaus, G.U. Nienhaus, Engineered nanoparticles interacting with cells: size matters, Journal of nanobiotechnology, 12 (2014) 5.

1